npj | flexible electronics

www.nature.com/npjflexelectron

ARTICLE OPEN

Check for updates

On-skin and tele-haptic application of mechanically decoupled taxel array on dynamically moving and soft surfaces

Se Young Kwon[1,5], Gyeongsuk Park[1,5], Hanbit Jin[2,5], Changyeon Gu[3], Seung Jin Oh[3], Joo Yong Sim[4], Wooseup Youm[2], Taek-Soo Kim[3], Hye Jin Kim[2]✉ and Steve Park[1]✉

To accurately probe the tactile information on soft skin, it is critical for the pressure sensing array to be free of noise and inter-taxel crosstalk, irrespective of the measurement condition. However, on dynamically moving and soft surfaces, which are common conditions for on-skin and robotic applications, obtaining precise measurement without compromising the sensing performance is a significant challenge due to mechanical coupling between the sensors and with the moving surface. In this work, multi-level architectural design of micro-pyramids and trapezoid-shaped mechanical barrier array was implemented to enable accurate spatiotemporal tactile sensing on soft surfaces under dynamic deformations. Trade-off relationship between limit of detection and bending insensitivity was discovered, which was overcome by employing micropores in barrier structures. Finally, in-situ pressure mapping on dynamically moving soft surfaces without signal distortion is demonstrated while human skin and/or soft robots are performing complicated tasks such as reading Braille and handling the artificial organs.

npj Flexible Electronics (2022)6:98 ; https://doi.org/10.1038/s41528-022-00233-0

INTRODUCTION

Over the past several decades, tactile sensors have attracted great attention due to their many exciting potential applications in wearable healthcare devices[1–3], robotics[4–8], prosthesis[9–12], human-machine interface[13–15], and augmented/virtual reality[16–21]. Pressure sensing in the form of a large array is especially important in realizing artificial tactile sensation, as it enables spatiotemporal pressure analysis similar to that of human skin[22].

However, the progress of pressure sensing array towards practical applications mentioned above is currently still hampered by several critical challenges. Firstly, the abovementioned applications often require pressure sensor array that functions properly on any surface, from soft biological tissues to elastomeric robotic skin, without compromising spatial accuracy. However, when pressure is applied on a soft material, deformation of the soft material inevitably occurs around the pressed region, which also deforms the sensors that has not been specifically pressed, thus generating unwanted noise and crosstalk in the signal output. This problem could be mitigated by inserting additional layer between taxels to isolate taxels; however, the additional layer decreases the pressure sensitivity by disrupting the deformation of sensing layers under pressure[23]. Developing an algorithm and data processing method can decrease crosstalk noise signals issue[24]; however, this requires pre-calibration and periodic recalibration, thus complicating the output signal acquisition.

Along with the above feature, the pressure sensor array should mechanically decouple pressure from other physical stimuli; in other words, it is critical that it is insensitive to other mechanical stimuli such as bending so that spatiotemporal information is reliably acquired on dynamically moving surfaces (which is often encountered in wearable devices and robotics) without compromising the performance of the pressure sensors. To address such a challenge, capacitive pressure sensors were shown to have negligible response to bending depending on the material[25] and geometrical design[26–28]. However, capacitive pressure sensors suffer from cross-capacitance noise as taxel density increases[24]. Pressure sensors based on piezoresistive materials are less prone to inter-taxel cross-talk, making them more attractive for array applications. A piezoresistive electrospun nanofibrous membrane was found to be insensitive to bending, attributed to its extremely small thickness[29]. However, the nanofibrous membrane limited the pressure detection range up to only 1 kPa, which is insufficient for detecting pressures needed in daily life. A carbon nanotube-coated microporous PDMS pressure sensor was also found to be bending insensitive due to the selective opening and closing behavior of its micropores[30]. However, the scaling down of taxels and large-area array fabrication has not been demonstrated. Detecting the change in the contact resistance between conductive microstructures and electrodes is another method to measure pressure[31]. In these sensors, by initially preventing contact between the two parts under bending using spacers, it would in principle be possible to impart bending insensitivity. However, changing the microstructural design to implement such a feature will likely compromise performance of the sensor. For example, since pressure is initially needed to make contact between the two parts, the limit of detection (LoD) will be compromised. Furthermore, it would also be difficult to maintain the same sensor property at various bending angles due to the structural change of the sensor. Therefore, there still remains a significant challenge of fabricating a sensor array that has the same high sensing functionality regardless of the softness and the motion of the surface, thus hindering practical tactile sensing applications.

Herein, we introduce contact resistance-based pressure sensor array technology based on multiscale microstructural design of

[1]Department of Materials Science and Engineering, Korea Advanced Institute of Science and Technology (KAIST), Daejeon 34141, Republic of Korea. [2]Electronics and Telecommunications Research Institute (ETRI), Daejeon 34129, Republic of Korea. [3]Department of Mechanical Engineering, Korea Advanced Institute of Science and Technology (KAIST), Daejeon 34141, Republic of Korea. [4]Department of Mechanical Systems Engineering, Sookmyung Women's University, Daejeon 04313, Republic of Korea. [5]These authors contributed equally: Se Young Kwon, Gyeongsuk Park, Hanbit Jin. ✉email: nolowara@etri.re.kr; stevepark@kaist.ac.kr

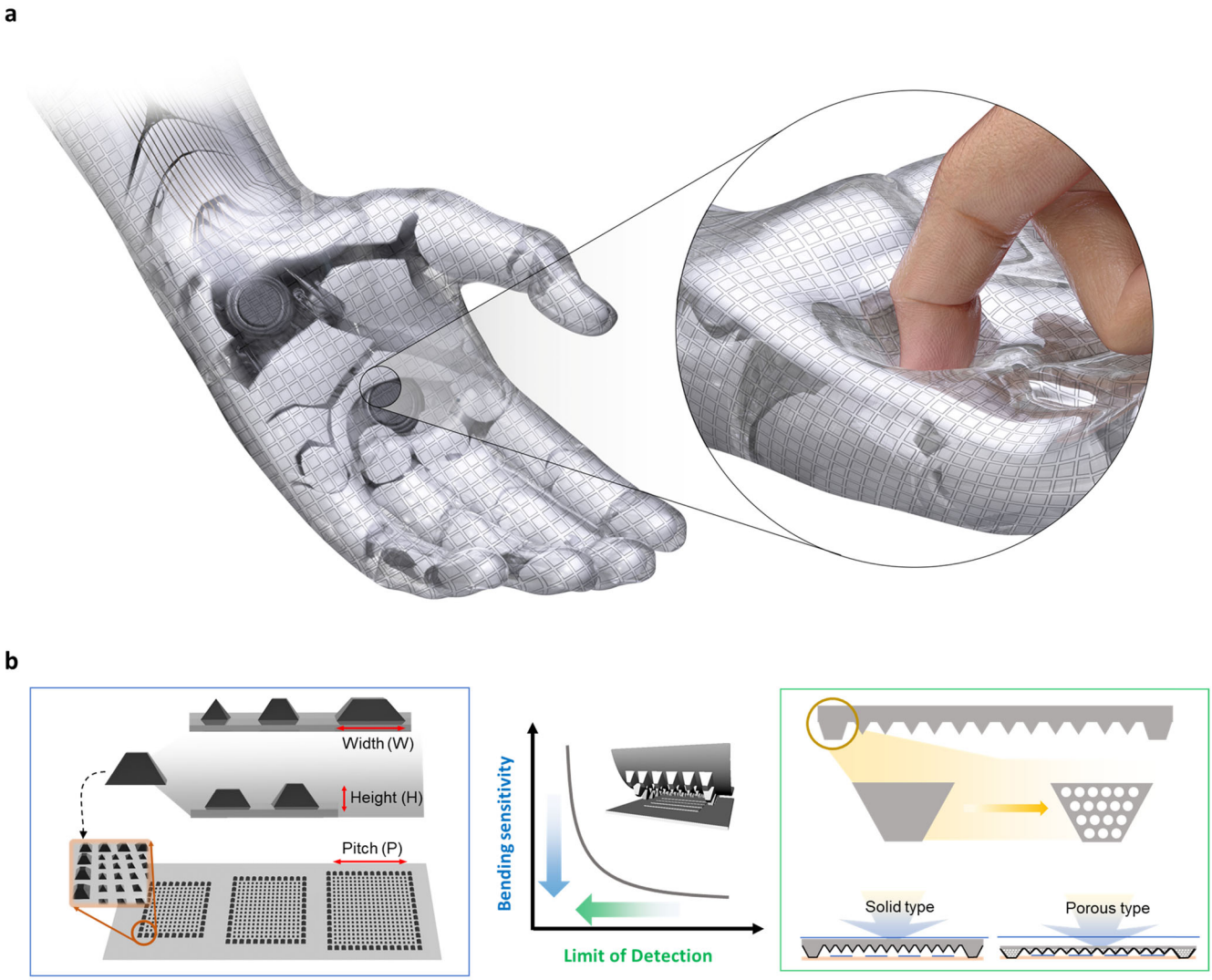

Fig. 1 Overall concept of MDPS. a Schematic illustration of MDPS application for soft robotics and electronics. **b** Illustration of the multiscale microstructures for optimizing bending insensitive property (left) and the introduction of porous structure to overcome the trade-off relationship between bending sensitivity and LoD.

micro-pyramids and trapezoid-shaped mechanical barrier array to enable accurate spatiotemporal pressure analysis with negligible mechanical cross-talk on surfaces of different modulus and on dynamically bending surfaces. Figure 1a is the overall schematic of our pressure sensor array depicted on a human or soft robotic hand. Through structural optimization of the mechanical barrier array, LoD (190 Pa) and bending sensitivity (insensitive down to a bending radius of 2.7 mm) were simultaneously minimized, as depicted in (Fig. 1b). Furthermore, the optimized multiscale microstructure was employed to a 12×12 large area pressure sensing array for a signal distortion-free spatiotemporal pressure mapping on a soft surface. To verify the practical usability of our pressure sensor array, various applications such as braille and letter recognition were demonstrated on soft and freely moving surfaces. Also, our sensor array was integrated with a soft robotic gripper for tele-medical application, handling delicate artificial organs and provided haptic feedback to a remotely placed actuator array. These demonstrations confirm the high utility and versatility of our sensor array for various tactile sensing applications, thus providing a pathway for rapid development and commercialization of tactile sensors.

RESULTS

Design and working mechanism of mechanically decoupled pressure sensor

The working mechanism of our contact-resistance based pressure sensor, which will be called mechanically decoupled pressure sensor (MDPS) from this point forward, is presented in Fig. 2a. Microstructured PDMS (Polydimethylsiloxane) coated with polypyrrole was used to make contact with interdigitated electrodes to alter the contact resistance (or equivalently conductance) with pressure (see Supplementary Figs. 1 and 2 for fabrication details and scanning electron microscopy (SEM) images, respectively). MDPS is designed with mechanical barrier array in the form of porous trapezoidal prism (TP) periodically placed along the periphery of the interdigitated electrodes while porous pyramid shaped microstructures resided directly on top of the electrodes. The heights of the TP were 70~140 μm and the height of pyramids were fixed to 70 μm while the diameter of the pores was 20 μm. A conventional design of pyramid shaped microstructure-based pressure sensor[32] (i.e. without the peripheral TP design nor porosity) was used as reference pressure sensor. On an un-curved flat surface, both the reference (top) and the MDPS (bottom) have considerably high contact resistance (R_c) since there is minimal

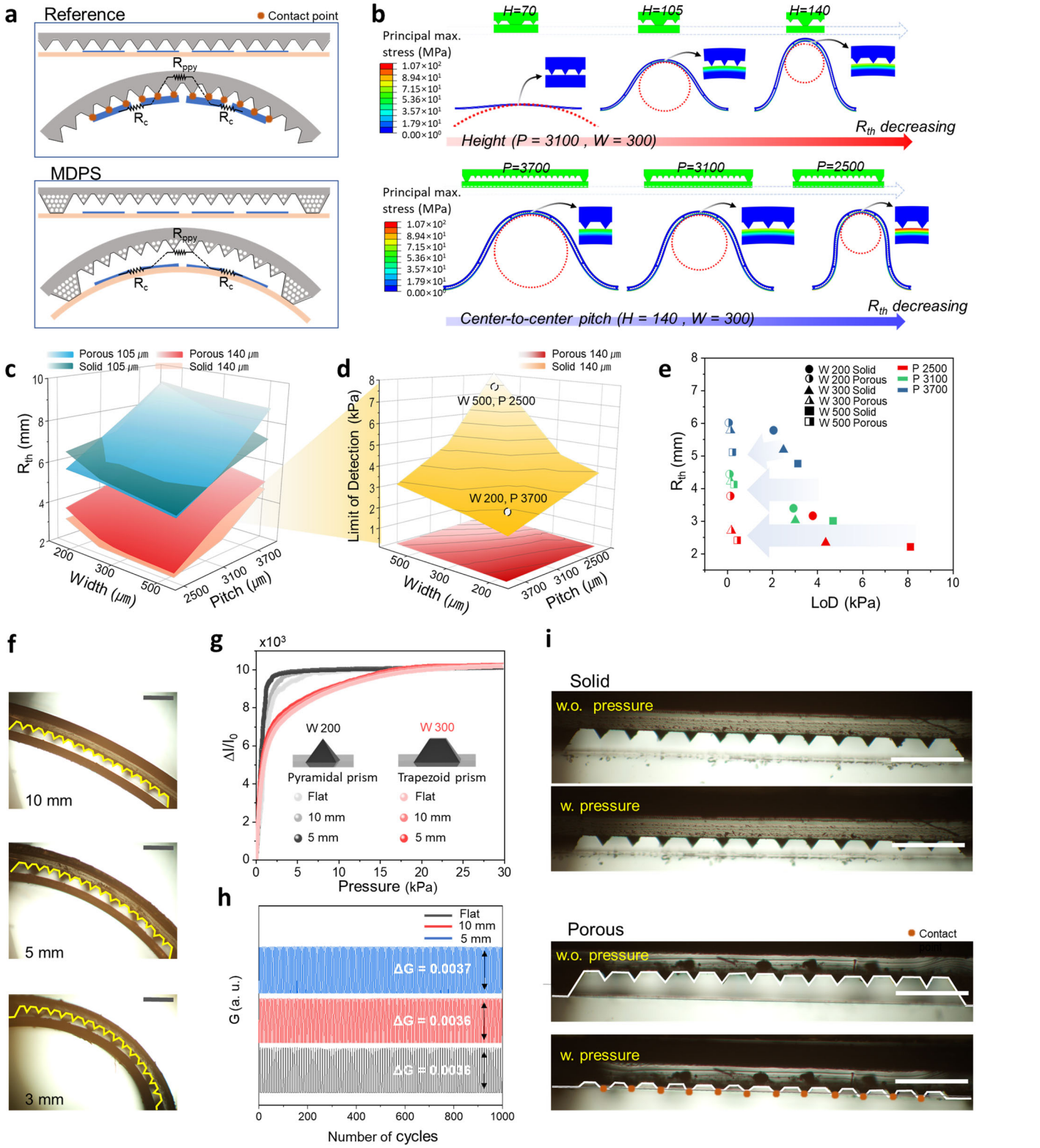

Fig. 2 Sensor characterization for the optimization of bending insensitivity and LoD. a Schematics of the reference and MDPS at the flat and bent surface. **b** Simulation results for various TP height and center-to-center pitch. **c** R_{th} values for the samples with varied TP variables. **d** LoD value comparison between porous and solid TP at the height of 140 μm. **e** Correlation between R_{th} and LoD with porosity. **f** Optical images of MDPS on surfaces with various bending radius. Scale bar, 500 μm. **g** Pressure response of MDPS with W 200 and 300 at the flat and bent condition with the various bending radius. **h** Repeated pressure cycle test on flat and bent surfaces showing constant change in conductance for any surfaces. **i** Optical images of MDPS with solid and porous TP under the pressure of 1 kPa. Scale bar, 500 μm.

physical contact between the microstructures and the electrodes. However, when the reference sensor is bent, lateral strain causes contacting of the pyramids with the electrodes, thus generating an unwanted decrease in R_c even without applied pressure. Hence, the reference sensor with the conventional designs collects the distorted mapping signals affected by both contact pressure and bending. However, in the case of MDPS, the trapezoidal prism array which has taller height than micro-pyramids prevent the contact between the pyramids and the electrodes under bending, thus enabling low distortion pressure mapping and bending insensitivity on soft and dynamically moving surfaces.

It is important to minimize the bending radius at which R_c begins to decrease (we will call this R_{th} from this point onward), as this determines the limit of how much the pressure sensor can be bent. To analyze the effect of TP geometry on R_{th}, numerical simulation was conducted using finite element method (built in ABAQUS) varying the height (H = 70, 105, 140 μm), center-to-center pitch (P = 2500, 3100, 3700 μm), and width (W = 300, 500 μm) (Fig. 2b and Supplementary Fig. 3a). The height, center-to-center pitch, and width were selected as the dominant parameters since they are directly related to the compressive modulus of TP while the pitch is related to the effective bending modulus sensor. R_{th} decreased with increasing height and width and with decreasing pitch, with height having a relatively greater effect followed by pitch and width, respectively (see Supplementary Fig. 3b for details).

To experimentally verify the trend observed in numerical simulation, pressure sensors with different geometries of porous and non-porous TP at various combinations of width (W = 200, 300, 500 μm), height (H = 105, 140 μm), and pitch (P = 2500, 3100, 3700 μm) were fabricated and their conductance were measured while being bent (see Supplementary Fig. 4a for experimental set up). Here, R_{th} was defined as the bending radius at which the conductance was 5% of the saturated conductance under extreme bending (Supplementary Fig. 4b)[30]. As depicted in Fig. 2c and Supplementary Fig. 5, R_{th} decreases with increasing height and width and with decreasing pitch, which was the trend observed in numerical simulation. It is also evident that height had the greatest influence on R_{th}, followed by pitch and width. The lowest R_{th} that was attained was 2.20 mm, at a height, width, and pitch of 140, 500, and 2500 μm, respectively. Porous and non-porous samples showed nearly identical trends with the porous samples having a slightly higher average R_{th} of 0.63 mm compared to that of non-porous samples.

The LoD of the sensors composed of porous and non-porous TP at different dimensions of width and pitch were measured, with the height fixed at 140 μm (see experimental section for details). LoD was defined as the pressure at which the conductance reached 3 times the noise level (Supplementary Fig. 6). As shown in Fig. 2d and Supplementary Fig. 7, in the case of non-porous TP, the effects of width and height show opposite trend towards LoD compared to that of R_{th} (i.e. LoD decreases with increasing pitch and decreasing width). Hence, there exists a trade-off between R_{th} and LoD as depicted previously in Fig. 1b; the abovementioned non-porous TP geometry that yielded minimal R_{th} of 2.20 mm has a relatively high LoD of 8.132 kPa. LoD of 2.06 kPa can be achieved at another TP geometry; however, the R_{th} here is relatively high at 5.78 mm.

Such a trade-off issue can be overcome with the introduction of micropores within the microstructures. Porous structure lowers the modulus of the structure[33], making it more easily compressible. Moreover, microporous structures exhibit innate bending insensitive property. When bent, a microporous structure rearranges its configuration to induce deformation throughout the entire structure. However, each micropores undergoes relatively small deformation with no significant distortion with the bridges surrounding the micropores even under the bending with the radius of 5 mm or smaller[30]. As a result, the microporous TP maintained its shape under bending and showed the similar bending insensitivity compared to the non-porous TP. As depicted in Fig. 2e and Supplementary Fig. 8, the LoD of the porous samples were lower by an average factor of 20 compared to that of non-porous sample with the same dimension while maintaining nearly the same bending insensitive properties. Figure 2f is the optical images of the sensor under bending (bending radius of 3, 5, 10 mm), showing that the pyramids had no contact with the electrodes until bending radius reached ~3 mm due to the bending insensitive nature of microporous structures.

As a means to select the optimal porous TP geometry to be used for various practical pressure sensing demonstrations, three samples with the lowest values of R_{th} were firstly selected, all of which had a pitch of 2500 μm. Here, sample with a TP width of 500 μm was not considered due to its relatively high LoD. We note here that R_{th} was measured without the application of pressure while LoD was measured without the sensor being bent. However, to ensure data reliability under practical applications, it is important to characterize the pressure sensing properties when both pressure and bending is applied simultaneously. Figure 2g is a plot of relative change in current as a function of pressure at various bending radii for the two remaining samples (TP width of 200 μm and 300 μm). For TP width of 200 μm with the pyramidal shape, the sensors characteristics changed at different bending radii; also, the sensor saturated rapidly at around 2 kPa. Porous pyramidal shape has relatively lower compressive modulus and therefore the pyramidal shaped TPs were compressed under bending exhibiting inconsistent sensor characteristics at different bending radii[33]. On the other hand, for TP width of 300 μm with the trapezoidal shape, the sensing characteristics remained consistent with a relatively large dynamic range over 20 kPa due to enhanced compressive modulus. Therefore, TP with a width of 300 μm (pitch of 2500 μm, height of 140 μm) was chosen as our optimal TP geometry. The characteristics of sensing properties from hereon is based on this TP geometry unless stated otherwise. The comparison table of major sensing performances were shown in Supplementary Table 1.

Cycling of our sensor at 3 kPa for 1000 cycles (Fig. 2h) showed similar characteristics under different bending radii (Flat, 5, 10 mm), furthermore confirming that bending does not affect the pressure sensing performance. Moreover, the response time and the relaxation time of the sensor were measured to be 12 ms and 6 ms, respectively (Supplementary Fig. 9). Figure 2i compares images of the non-porous and porous samples under 1 kPa of pressure. Under pressure, the pyramids of the non-porous sample did not contact the electrodes; whereas, the contact was clearly made for the porous sample, corroborating the experimental data.

Characterization of sensor array on soft dynamic surfaces

An array of 12 × 12 MDPS (array and individual taxel with an area of 4225 and 2.21 mm^2, respectively) was fabricated by placing the porous microstructure on top of interdigitated electrodes patterned on flexible PCB, which was then encapsulated with a medical tape, 3 M Tegaderm (Fig. 3a). The fabricated arrays had uniform characteristics, as seen in Supplementary Fig. 10. Conventional pyramid-based sensor array was used as a reference for comparison. Firstly, the reference and the MDPS sensor array were bent to various bending radii from 5 to 20 mm along different bending axis, and the number of taxels with an output signal were counted. As shown in (Fig. 3b), MDPS array was insensitive to bending deformation showing zero responding taxels irrespective of bending radii and bending axis. However, the reference array showed high sensitivity to bending with an average of 16, 29.7, and 40.7 responding taxels at bending radius of 20, 10, and 5 mm, respectively. This confirms that bending insensitivity of MDPS also translates to arrays.

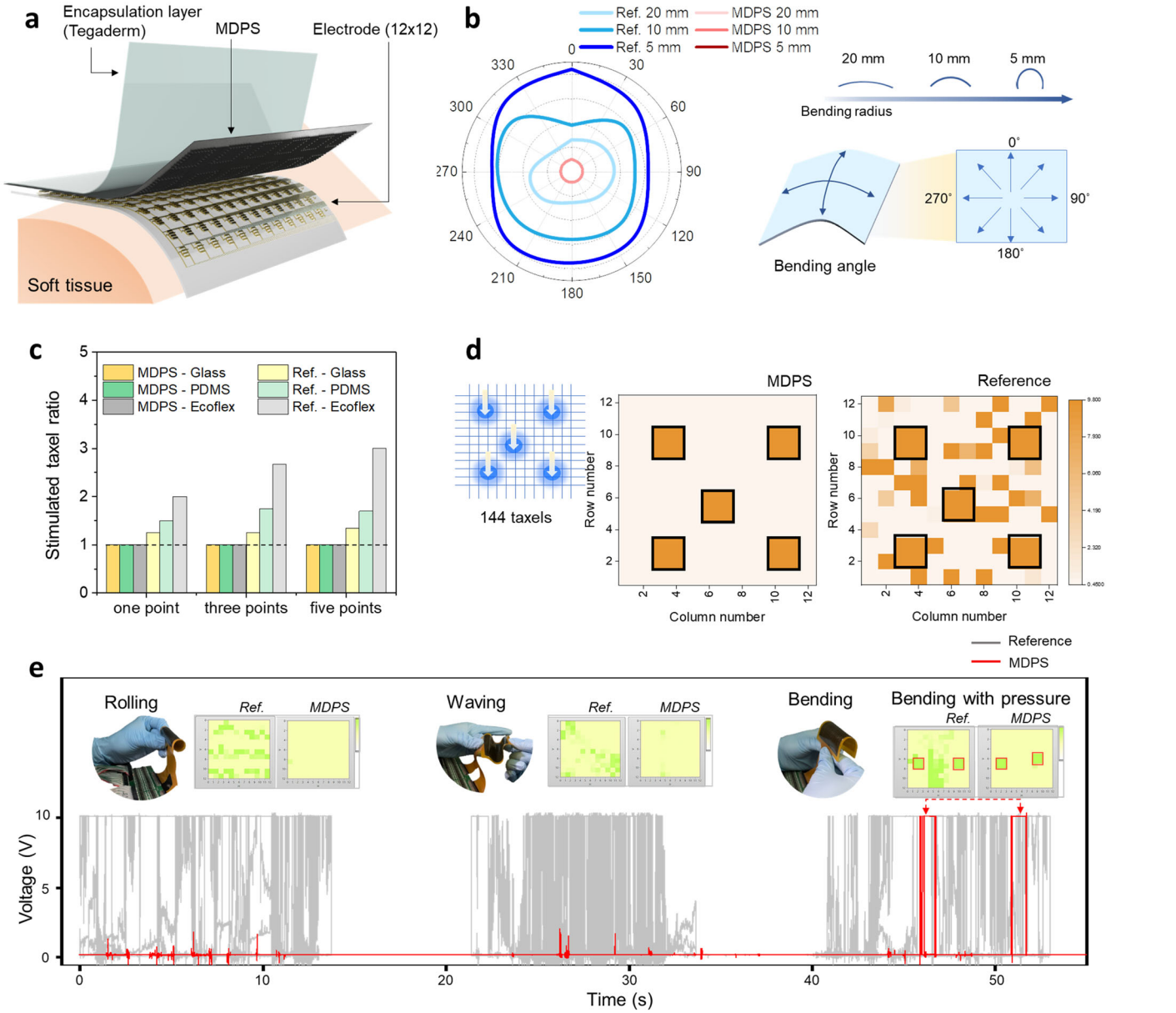

Fig. 3 12 ×12 MDPS array characterization on soft surface. a Schematic illustration of MDPS array integrated with flexible 12 × 12 electrode. **b** Stimulated taxel numbers along bending directions and angles. **c** Stimulated taxel ratio of multipoint measurement according to the modulus of substrates. **d** Visualized taxel images of reference and MDPS when five points were pressed on the Ecoflex. **e** Responsiveness of reference and MDPS array under dynamic deformations such as rolling, waving, and bending.

As mentioned in the introduction, spatial accuracy of pressure data on various surfaces is important for versatile applicability of tactile sensors. In this regard, MDPS and reference array were placed on various substrates with varying modulus: glass, PDMS, and Ecoflex, as shown in Supplementary Fig. 11. For each of the six cases, contact was made at 1, 3, and 5 different positions simultaneously (each contact point pressed 4 taxels), yielding a total of 18 data points as seen in Fig. 3c. Stimulated taxel ratio is defined as the number of stimulated taxels (i.e. taxels with a signal change) divided by the intended pressed taxels (i.e. 4, 12, 20 taxels). In the case of MDPS array, regardless of the surface, the expected number of taxels were stimulated, yielding stimulated taxel ratio of 1. However, in the case of reference array, the type of surface strongly dictated the number of stimulated taxels. For Ecoflex in particular (the substrate with the lowest modulus), 8, 34, and 60 taxels were stimulated (yielding stimulated taxel ratio of 2.00, 2.83, and 3.00) respectively. Figure 3d and Supplementary Fig. 12 depict array graphics, clearly showing that for the reference array, significant mechanical crosstalk is present on Ecoflex. This result also firmly shows that even though the area surrounding the pressed region is deformed, the structural design of MDPS array effectively discretizes the mechanically coupled taxels, thus causing only the pressed taxels to be deformed.

In practical settings, sensors placed on soft surfaces undergo complex dynamic bending rather than them being statically bent. Real-time monitoring of 12 × 12 MDPS array under various types of dynamic motion such as bending, waving, rolling were demonstrated and the voltage signals from 144 taxels are plotted in Fig. 3e. The reference array sensitively responded to rolling, waving, and bending; hence, when pressure was applied under these dynamic circumstances, pressure could not be measured. On the other hand, MDPS array demonstrated negligible noise

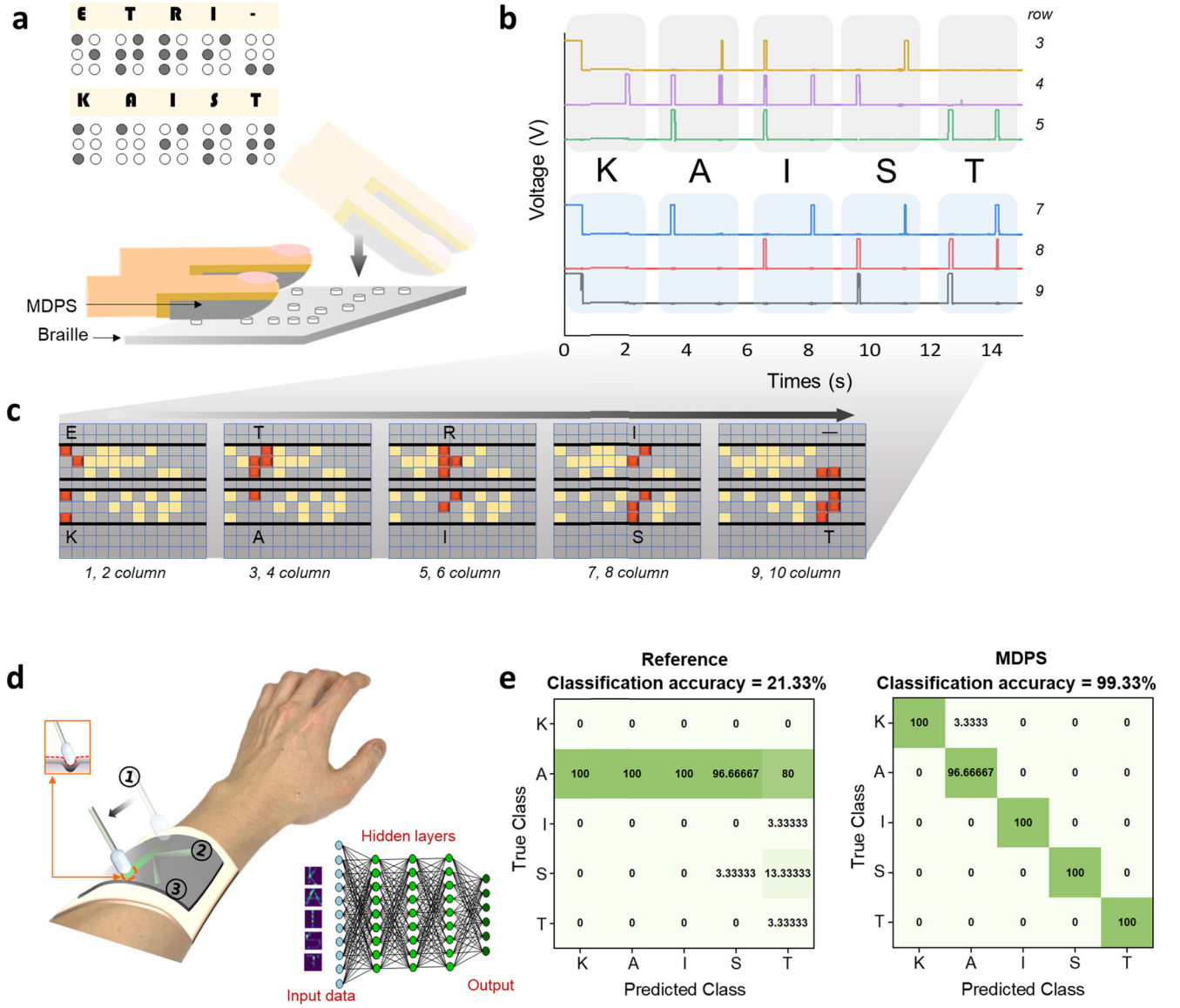

Fig. 4 On-skin application demonstration. a Schematic illustration of braille recognition with MDPS. **b** Acquired voltage signals from MDPS while an user reads braille letters ETRI-KAIST. **c** Sequentially visualized pressed taxels while reading the braille letters. **d** Schematic illustration of MDPS for the letter recognition on a forearm. **e** Classification accuracies of reference and MDPS of letter recognition through machine-learning based on convolutional neural network.

under the various forms of dynamic motion, and only responded to applied pressure (Supplementary Video 1).

Demonstration of on-skin applications

The high sensing performance of MDPS array on soft surfaces along with bending insensitivity enables precise measurement of pressure on human skin. We demonstrated two on-skin applications each utilizing the distinctive features of MDPS array. Firstly, braille reading was demonstrated by attaching 3×12 taxel arrays on two fingers (long axis along the length of the fingers) with a bending radius of 5 mm. Braille pattern was analyzed sequentially by stimulating 6 taxels at a time, via applying pressure starting at the finger tips and down onto the other end of the fingers. Each dot in the Braille pattern had a size of 1 mm^2. Total 10 braille letters that spells out ETRI-KAIST were read by MDPS array (Fig. 4a). Attributed to the small size of each taxel (2.21 mm^2), spatial decoupling of the taxels, and bending insensitivity, clear and distinctive taxel stimulation analogous to the braille pattern was observed, as depicted in Fig. (4b and c).

As a second on skin application, a 12×12 MDPS array was placed on a forearm (a curved soft human tissue), letters were traced out using a round-ended rod, and machine learning based on convolutional neural network (i.e., 2 consecutive blocks of 3×3 convolution and 2×2 max-pooling, followed by 3×3 convolution and two fully connected layers of 150 and 5 neurons) was utilized to recognize the letters. The word "KAIST" were written 30 times to use as training data and the trained data were validated with the additional 150 times of the letter recognition (Fig. 4d). As seen in the confusion matrix plot in Fig. 4e, MDPS array exhibited superior predictive accuracy of 99.33%; whereas, that of the reference array exhibited a low accuracy of 21.33%. Such a difference in the accuracy is again attributed to the spatial mechanical decoupling of each taxel and the bending insensitivity of the MDPS array.

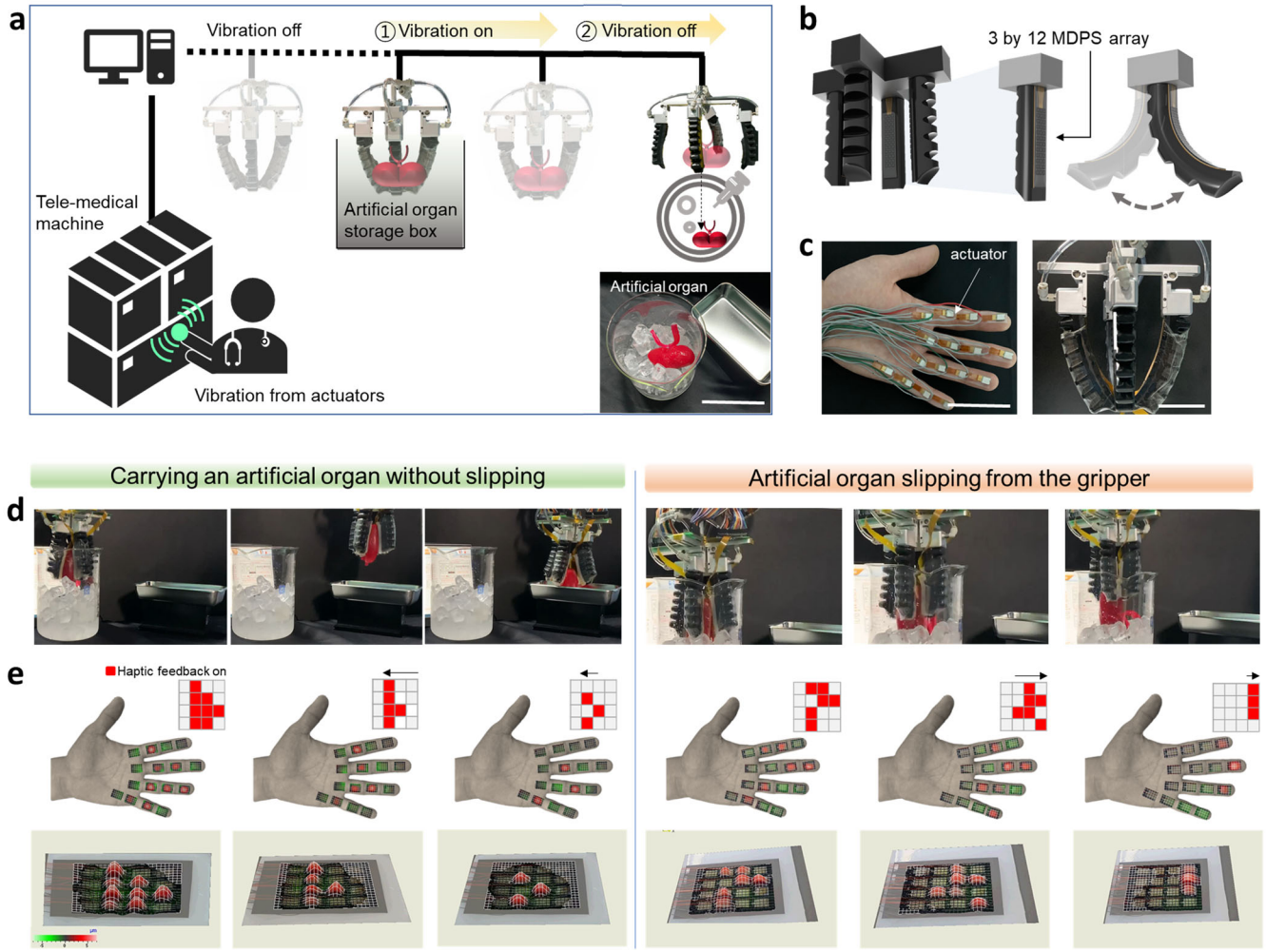

Fig. 5 Tele-haptic system demonstration. a Schematics of integrated tele-haptic system interacting operators and soft grippers. Real image of an artificial organ in the storage box (inset). Scale bar, 10 cm. **b** Schematics of MDPS attached on a soft gripper with 4 fingers. **c** Photos of actuators and the pneumatic soft gripper. Scale bars, 5 cm. **d** Sequential images of two different tele-medical situations. **e** Displacement of vibrating actuators tracked by laser scanning vibrometer under operation.

Demonstration of tele-haptic application

Finally, we demonstrated a tele-haptic system that enables remote operation by providing spatially distributed haptic feedback to user during the careful handling of fragile object such as artificial organs. The system consists of a soft gripper with MDPS array, which could gather accurate spatiotemporal tactile information while carrying an artificial organ, and a remotely placed soft robot control system, which provides haptic feedback for an operator to recognize the status of gripping (Fig. 5a). As shown in Fig. 5b and c, four sets of 3×12 MDPS arrays were attached to each of 4 fingers of the pneumatic soft gripper, and the spatiotemporal pressure mapping information was transmitted to 4×4 actuating array to provide the haptic feedback to a distant operator. Each actuator was assigned to 9 taxels of MDPS and the actuator was activated if the pressure detected from the assigned taxels exceeded the preset threshold (Supplementary Fig. 13).

Two different tele-medical situations were demonstrated with the tele-haptic system; in the former case, an artificial organ was tightly gripped and properly carried to a surgical dish. For the latter case, an organ slipped through the gripper during the operation. (Fig. 5d and Supplementary video 2, 3). For each situation, the 4×4 actuator array generated spatially distributed vibration according to the pressure distribution measured from MDPS on the soft gripper, and the displacement of vibrating actuators on the hand-shaped feedback transmission device was measured with 3D laser scanning vibrometer and displayed as a color heatmap in Fig. 5e. For both situations, the initial firm grasping of the artificial organ provided haptic feedback with steady vibrations from the turned-on actuators. However, the sequence of how haptic feedback vanishes was different for each condition. As shown in three images on the left side of (Fig. 5e), when an organ was properly carried without slipping and safely dropped on a surgical dish, the haptic feedback sequence started vanishing from fingertip since the pneumatic gripper opens from its fingertip where the contact is initially lost. However, when an organ slipped from the gripper due to its slippery surface, the haptic feedback start vanishing in the opposite direction, from palm to fingertip, as shown in the three right images in (Fig. 5e). In both situations, the MDPS and actuators did not respond to the bent grippers before and after grasping the artificial organ. This demonstration showed that this tactile sensitive gripper can detect pressure regardless of bending with dynamic movements such as swaying while carrying the artificial organ, and therefore, confirmed the feasibility of MDPS for practical tele-medical applications.

DISCUSSION

Forthcoming practical tactile sensing applications will require pressure sensor arrays with high pressure detection accuracy on

soft surfaces that is constantly under motion. In this work, a trade-off relationship between limit of detection (a key performance figure of merit in tactile sensing) and limit of bending insensitivity in microstructure-based contact resistance pressure sensors was discovered. Such a trade-off was overcome by introducing porous trapezoidal prism-based spacers with optimized geometry. Trends observed in numerical simulation were in agreement with experimental results. The optimized sensor exhibited high pressure sensing performance simultaneously with bending insensitivity. The sensor array was also confirmed to be able to detect pressure with no signal crosstalk on soft surfaces and withstand various types of deformations including rolling and waving. To verify the sensor array's practical feasibility, it was attached on a finger and forearm for braille reading and machine learning-based letter recognition, respectively. Furthermore, a tele-haptic system that transmits the tactile sensation between a soft robot and a user was demonstrated, where accurate tactile signal transmission was possible due to the sensor's proper functionality on soft bending surfaces. We expect that the presented features of our sensor array and along with the demonstrations will pave the way for rapid advancement of pressure sensing arrays for various applications in human-machine interface, virtual/augmented reality, wearable electronics, and soft robotics in the near future.

METHODS

Fabrication of MDPS sensor array

A microstructured PDMS film was fabricated using a replica molding process, i.e., soft photolithographic molding. A silicon wafer was etched using potassium hydroxide (KOH) solution to form micro-pyramid structures with a side wall angle of 54.7°. The width and the gap of the micropyramids are both 100 μm, and the dimension of the truncated pyramids were mentioned in the manuscript. To employ porous structure, polystyrene (PS) beads with the diameter of 20 μm were filled into the silicon wafer using blade coating. MDPS was prepared by spin-coating PDMS on the trichloro(1H,1H,2H,2H-perfluorooctyl)silane -treated PS beads-filled wafer at 500 rpm for 30 s and heated in a convection oven at 80 °C for 2 h. The thickness of the as-fabricated PDMS film was 270 μm at the 140 μm-tall TPs and 200 μm at the 70 μm-tall micropyramids at the center. Next, cured PDMS film were immersed in a toluene (99%, Sigma Aldrich) and bath sonicated for 6 hours to thoroughly dissolve PS beads, and washed by ethanol and distilled (DI) water respectively to completely wash toluene. Polypyrrole (Pyrrole (98%), Sigma Aldrich) was then chemically grafted on the porous micropyramid film with the truncated pyramids as conventional chemical oxidation polymerization method[34]. Firstly, PDMS was treated using oxygen plasma chamber with 80 W power for 1 min and sealed with a 10 μl of pyrrole monomer silane (N-(3-trimethoxysilylpropyl)pyrrole, Alfa Chemistry) and heated to 80 °C for 45 min. The pyrrole was then polymerized in a 90 ml of aqueous solution mixture of 600 μl of pyrrole and 600 mg of oxidant solution (iron (III) p-toluene sulfonate hexahydrate, Sigma Aldrich) at room temperature. After the polymerization, the sample was washed with DI water using a bath sonicator. After grafting polypyrrole, the porous microstructured PDMS film was integrated with a 4-finger interdigitated electrode (i.e., the length and width of each finger are 1500 and 100 μm, and the gap between fingers is 300 μm) on a flexible polyimide substrate using tegaderm (purchased from 3 M) as encapsulating layer. The surface and cross-sectional morphologies of the MDPS were characterized by optical microscopy and field-emission scanning electron microscopy (FE-SEM, Hitachi s4800).

Finite element simulation for understanding bending insensitivity

Finite element analysis was performed using ABAQUS/CAE to analyze the trend of bending insensitivity of MDPS depending on the spacer height and spacer-to-spacer distance. The model consists of three parts: a polyimide (PI) substrate, a PDMS with pyramids and spacers on the PI substrate, and a rigid circular body for the initial bending step. Linear elastic and isotropic materials properties were used for PI (Young's modulus: 3.0 GPa, Poisson's ratio: 0.34) and PDMS (Young's modulus: 2.6 MPa, Poisson's ratio: 0.49). The total number of quadrilateral elements was 62000–95446 depending on the types of MDPS. To give an upward bending motion of the\ a small displacement was applied to the rigid circular body at the initial step. Then, a right-sliding motion of the left edge of the MDPS was applied linearly until the pyramids of the PDMS contact with the PI substrate. The bending insensitivity was derived based on the bending radius, which was calculated when the pyramids of PDMS first contact with the PI substrate.

Sensor characterization

TP was pressed by z-axis force gauge with the tip size of 5 × 5 mm. LoD of samples were measured by a load cell pressure measurement station with DAQ board, applying a bias voltage of 2 V from power supply (E3631A, Keysight), a low-noise current preamplifier (SR570, Stanford Research Systems), and a force gauge (PI V-275.431, force range of 0.01 N to 10 N and resolution of 0.001 N (0.01 gf)). 3 × 3 MDPS array was placed in a high-precision universal equipment (EMS 303) using clamps. Z-axis stage was controlled with a resolution of 10 μm and the conductivity of the center taxel was measured using a LCR meter (HP4284A).

MDPS array measurements

The resistance changes of MDPS array were measured by preamplifier circuits and a data acquisition system (NI DAQ, USB-6255, National Instruments). 12 × 12 MDPS array are connected to the 144-channel preamplifier circuit which is composed of voltage divider and follower circuits for converting the resistance changes to output voltage. And the data was visualized by color heat map by using LabView program.

Laser scanning vibrometer

The characteristics of the actuator array were investigated using a laser scanning vibrometer (LSV) system (PSV-400, PolyTech GmbH, Germany) with a laser scanning head (PSV-400), a scanning vibrometer controller (OFV-5000), and a junction box (PSV-400).

Tele-medical application

The acquired datasets of 12 × 12 MDPS array (pressure maps) were assigned to 4 × 4 actuator array to provide spatially distributed haptic feedbacks. The actuator array is made of 6 mm× mm size multilayered piezoelectric actuators. And the input voltage of 40 V_{pp} (200 Hz sine wave) was applied to actuator by using piezo amplifier (E-663, PI).

Statistical analysis

For Supplementary Figures 5 and 7, the standard deviation was calculated using $s = \sqrt{\frac{\sum_{i=1}^{N}(x_i - \bar{x})^2}{N-1}}$, where s is the standard deviation, N is the number of sample measurements ($N = 10$), and $\bar{x}$ is the mean value of the measurements.

DATA AVAILABILITY

All data are available in the main text or Methods. The data that support the findings of this study are available from the corresponding author upon reasonable request.

Received: 14 September 2022; Accepted: 8 December 2022;
Published online: 21 December 2022

REFERENCES

1. Kaisti, M. et al. Clinical assessment of a non-invasive wearable MEMS pressure sensor array for monitoring of arterial pulse waveform, heart rate and detection of atrial fibrillation. *NPJ Digit. Med.* **2**, 39 (2019).
2. Yang, J. et al. Eardrum-inspired active sensors for self-powered cardiovascular system characterization and throat-attached anti-interference voice recognition. *Adv. Mater.* **27**, 1316–1326 (2015).
3. Zhu, P. et al. Skin-electrode iontronic interface for mechanosensing. *Nat. Commun.* **12**, 4731 (2021).
4. Cataldi, P. et al. Carbon nanofiber versus graphene-based stretchable capacitive touch sensors for artificial electronic skin. *Adv. Sci.* **5**, 1700587 (2018).
5. Jin, T. et al. Triboelectric nanogenerator sensors for soft robotics aiming at digital twin applications. *Nat. Commun.* **11**, 5381 (2020).
6. Lee, W. W. et al. A neuro-inspired artificial peripheral nervous system for scalable electronic skins. *Sci. Robot.* **4**, eaax2198 (2019).
7. Núñez, C. G. et al. Energy-autonomous, flexible, and transparent tactile skin. *Adv. Funct. Mater.* **27**, 1606287 (2017).
8. Truby, R. L. et al. Soft somatosensitive actuators via embedded 3D printing. *Adv. Mater.* **30**, 1706383 (2018).
9. Kim, J. et al. Stretchable silicon nanoribbon electronics for skin prosthesis. *Nat. Commun.* **5**, 5747 (2014).
10. Wu, Y. Z. et al. A skin-inspired tactile sensor for smart prosthetics. *Sci. Robot.* **3**, eaat0429 (2018).
11. Kwak, J. W. et al. Wireless sensors for continuous, multimodal measurements at the skin interface with lower limb prostheses. *Sci. Transl. Med.* **12**, eabc4327 (2020).
12. Osborn, L. E. et al. Prosthesis with neuromorphic multilayered e-dermis perceives touch and pain. *Sci. Robot.* **3**, eaat3818 (2018).
13. Tao, J. et al. Self-powered tactile sensor array systems based on the triboelectric effect. *Adv. Funct. Mater.* **29**, 1806379 (2018).
14. Sim, K. et al. Metal oxide semiconductor nanomembrane-based soft unnoticeable multifunctional electronics for wearable human-machine interfaces. *Sci. Adv.* **5**, eaav9653 (2019).
15. Tan, H. et al. Tactile sensory coding and learning with bio-inspired optoelectronic spiking afferent nerves. *Nat. Commun.* **11**, 1369 (2020).
16. Yu, X. et al. Skin-integrated wireless haptic interfaces for virtual and augmented reality. *Nature* **575**, 473–479 (2019).
17. Oh, J. et al. A liquid metal based multimodal sensor and haptic feedback device for thermal and tactile sensation generation in virtual reality. *Adv. Funct. Mater.* **31**, 2007772 (2020).
18. Kim, K. K. et al. A deep-learned skin sensor decoding the epicentral human motions. *Nat. Commun.* **11**, 2149 (2020).
19. Mishra, S. et al. Soft, wireless periocular wearable electronics for real-time detection of eye vergence in a virtual reality toward mobile eye therapies. *Sci. Adv.* **6**, eaay1729 (2020).
20. Lee, Y. et al. Soft electronics enabled ergonomic human-computer interaction for swallowing training. *Sci. Rep.* **7**, 46697 (2017).
21. Ge, J. et al. A bimodal soft electronic skin for tactile and touchless interaction in real time. *Nat. Commun.* **10**, 4405 (2019).
22. Oh, H. et al. Scalable tactile sensor arrays on flexible substrates with high spatiotemporal resolution enabling slip and grip for closed-loop robotics. *Sci. Adv.* **6**, eabd7795 (2020).
23. Bae, K. et al. Large-area, crosstalk-free, flexible tactile sensor matrix pixelated by mesh layers. *ACS Appl. Mater. Interfaces* **13**, 12259–12267 (2021).
24. Shao, R. et al. Crosstalk-free, stretching-insensitive sensor based on arch-bridge architecture for tactile mapping with parallel addressing strategy toward million-scale-pixels processing. *Adv. Sci.* **8**, e2101876 (2021).
25. Yoo, J.-Y. et al. industrial grade, bending-insensitive, transparent nanoforce touch sensor via enhanced percolation effect in a hierarchical nanocomposite film. *Adv. Funct. Mater.* **28**, 1804721 (2018).
26. Won, D.-J., Yoo, D. & Kim, J. Effect of a microstructured dielectric layer on a bending-insensitive capacitive-type touch sensor with shielding. *ACS Appl. Electron. Mater.* **2**, 846–854 (2020).
27. Yoo, D. et al. Double side electromagnetic interference-shielded bending-insensitive capacitive-type flexible touch sensor with linear response over a wide detection range. *Adv. Mater. Technol.* **6**, 2100358 (2021).
28. Su, Q. et al. A stretchable and strain-unperturbed pressure sensor for motion interference-free tactile monitoring on skins. *Sci. Adv.* **7**, eabi4563 (2021).
29. Lee, S. et al. A transparent bending-insensitive pressure sensor. *Nat. Nanotechnol.* **11**, 472–478 (2016).
30. Kim, S. et al. Wearable, ultrawide-range, and bending-insensitive pressure sensor based on carbon nanotube network-coated porous elastomer sponges for human interface and healthcare devices. *ACS Appl. Mater. Interfaces* **11**, 23639–23648 (2019).
31. Jk O'Neill, S. et al. A carbon flower based flexible pressure sensor made from large-area coating. *Adv. Mater. Interfaces* **7**, 2000875 (2020).
32. Mannsfeld, S. C. B. et al. Highly sensitive flexible pressure sensors with microstructured rubber dielectric layers. *Nat. Mater.* **9**, 859–864 (2010).
33. Yang, J. C. et al. Microstructured porous pyramid-based ultrahigh sensitive pressure sensor insensitive to strain and temperature. *Acs Appl. Mater. Interfaces* **11**, 19472–19480 (2019).
34. Oh, J. et al. Highly uniform and low hysteresis piezoresistive pressure sensors based on chemical grafting of polypyrrole on elastomer template with uniform pore size. *Small* **15**, 1901744 (2019).

ACKNOWLEDGEMENTS

This work was supported by Institute for Information & Communications Technology Promotion (IITP) grant funded by the Korea government (MSIT, Grant No. 2020-0-00003, Development of high piezoelectric coefficient composite and ultra-low power multilayered piezoelectric sensor/actuator multi-functional module, Grant No.2022-0-00025, Development of soft-suit technology to support human motor ability, and Grant No. 2022-0-00020, Imperceptible on-skin sensor devices for musculoskeletal monitoring and rehabilitation), and the KAIST UP Program.

AUTHOR CONTRIBUTIONS

S.Y.K., G.S.P., and H.J. are co-first authors. S.Y.K., G.S.P., and H.J. designed the experiments; S.Y.K. and G.S.P. prepared and conducted the experiments; H.J. and W.Y. analyzed the tele-haptic experiment. C.G. and S.J.O conducted the finite element simulation and the results was supervised by T.-S.K.; J.Y.S contributed to the on-skin letter recognition using machine learning; S.Y.K, G.S.P and S.P wrote the paper; S.P and H.J.K supervised the project and all authors contributed to the general discussion.

COMPETING INTERESTS

The authors declare no competing interests.

ADDITIONAL INFORMATION

Supplementary information The online version contains supplementary material available at https://doi.org/10.1038/s41528-022-00233-0.

Correspondence and requests for materials should be addressed to Hye Jin Kim or Steve Park.

Reprints and permission information is available at http://www.nature.com/reprints

Publisher's note Springer Nature remains neutral with regard to jurisdictional claims in published maps and institutional affiliations.